Magnetism in polycrystalline cobalt-substituted zinc oxide

A. S. Risbud,* N. A. Spaldin,† Z. Q. Chen, S. Stemmer,‡ and Ram Seshadri§
Materials Department, University of California, Santa Barbara, California 93106, USA
(Received 2 June 2003; published 5 November 2003)

We present results of the preparation (by precursor decomposition), characterization (with x-ray diffraction, transmission electron microscopy, and dc magnetization measurements), and detailed computation (using density functional theory) of polycrystalline ZnO with up to 15% substitution of the zinc sites by divalent cobalt. The experimental results indicate the dominant magnetic interaction in *well-characterized* stoichiometric phases $Zn_{1-x}Co_xO$, $x=0.05$, 0.10, 0.15, is nearest-neighbor antiferromagnetic. Our computations suggest robust ferromagnetism will only occur in the presence of additional hole doping.

DOI: 10.1103/PhysRevB.68.205202 PACS number(s): 75.50.Pp, 75.60.−d, 71.20.−b

I. INTRODUCTION

The emerging paradigm of spintronics[1]—solid-state electronics based on the spin property of the electron rather than the property of charge which is traditionally exploited—has provided the impetus for investigation of so-called dilute magnetic semiconductors (DMS's). One of the materials at the focus of much recent attention is the wide-band-gap wurtzite-phase semiconductor ZnO, in which some of the zinc can be substituted by magnetic transition-metal (TM) ions to yield a metastable solid solution. In many of these systems, it is believed that ferromagnetic coupling between TM ions can be achieved even in the limit of concentrations as low as 5%. This suggests the possibility of transparent ferromagnets, with potential application in magneto-optical devices. For example, Dietl *et al.*[2] have set up Ginzburg-Landau free-energy functionals in the magnetization for a number of manganese-substituted zinc-blende and wurtzite semiconductors. They find that 5% Mn substitution and some hole doping [$\mathcal{O}(10^{20})$ cm^{-3}] yields ferromagnetic coupling between the Mn spins. Curie temperatures are suggested to approach 300 K in Mn-substituted ZnO.

Sato and Katayama-Yoshida[3] used density functional theory within the Korringa-Kohn-Rostoker (KKR) and local spin density approximations to predict magnetic ground states for a range of ZnO:t*M* systems.[3] Their calculations on four unrelaxed ZnO unit cells (8 formula units) with 25% TM substitution favored a ferromagnetic ground state for most 3*d* TM's with the exception of Mn. For $Zn_6Mn_2O_8$, they find that hole doping induces ferromagnetism. These authors[4] have recently extended their study to lower TM concentrations and reached the same conclusions.

Experiments on thin films of ZnO:t*M* have been the subject of a number of recent papers—in particular, films made using the technique of pulsed laser deposition (PLD). In thin films of ZnO:t*M* (t*M*=Mn, Co, Ni, Cu) Ando *et al.*[5,6] find evidence for a significant influence of TM's on ZnO states in terms of a large magnetic circular dichroism signal at an energy corresponding to the ZnO band edge. Ueda *et al.*[7] find that PLD films of $Zn_{1-x}Co_xO$ with ($0.05\leqslant x\leqslant 0.25$) display Curie temperatures between 280 K and 300 K, and the films show a saturation magnetization between $1.8\mu_B$ and $2.0\mu_B$ per Co. Apart from the possibility of ''intrinsic'' ferromagnetism from $Zn_{1-x}Co_xO$, perhaps in the presence of hole carriers, it is suggested that sources of ferromagnetism could include the presence of cobalt oxide grains. Kim *et al.*[8] have used PLD to grow $Zn_{1-x}Co_xO$ and found evidence for ferromagnetism when the films are grown under low O_2 partial pressures, the origins of which are not ''intrinsic'' however, but due to the formation of cobalt microclusters. Laser molecular beam epitaxy has been used by Jin *et al.*[9] to grow ZnO:Co films (with some Al) on sapphire. Optical studies confirm Co is divalent, high spin, and substituting for Zn. Lim *et al.*[10] report ferromagnetism in $Zn_{1-x}Co_xO$ ($0.02\leqslant x\leqslant 0.40$) films grown by magnetron cosputtering on sapphire. In view of some of these results, a recent review of DMS state of the art by Pearton *et al.*[11] emphasizes the ZnO:Co system as particularly promising for applications requiring ferromagnetism near room temperature.

Stoichiometry and phase purity can be difficult to establish in thin films. Because of inaccuracies in estimating the concentration of magnetic ions, determining the precise nature of the magnetic coupling can also be difficult. Under metastable preparation conditions, it is known that the wurtzite ZnO lattice can stabilize up to 70% Co before evidence for phase segregation manifests.[12] This has encouraged us to pursue the examination of *bulk* polycrystalline samples of $Zn_{1-x}Co_xO$. In bulk samples, the uncertainties and inaccuracies in characterization are significantly diminished and a clearer picture of the magnetism which facilitates comparison with calculations emerges. To this end, we report a study of $Zn_{1-x}Co_xO$ using dc magnetic measurements on bulk samples and density functional calculations. Our studies suggest that in the absence of any other dopant, the $Zn_{1-x}Co_xO$ system is characterized by nearest-neighbor antiferromagnetic coupling between magnetic ions and that cooperative magnetism reflects the simultaneous coexistence of near-neighbor pairs of Co^{2+} ions along with ''isolated'' Co^{2+} ions.

The interpretation of our experimental data is guided by the results of our density functional calculations on 32-atom wurtzite ZnO supercells (16 ZnO units) with 1 and 2 Co atoms substituting for Zn. This corresponds to substitution levels of 6.25% and 12.5%, which are within the experimental range described here. The influence of hole and electron doping on the magnetic properties has been modeled by simply removing a Zn or O atom from the lattice. The results of the computation indeed support our primary conclusion that

 ©2003 The American Physical Society

robust ferromagnetism does not occur in Co-substituted ZnO, unless additional dopants which provide *p*-type carriers are also present.

II. EXPERIMENT

Since the system $Zn_{1-x}Co_xO$ is intrinsically metastable, a single-source precursor where these ions are already intimately mixed is desirable. Mixed metal oxalates fit the bill. In addition, they decompose in a clean manner to give metal oxides and the gaseous products water, CO, and CO_2. The mixed oxalate precursors $Zn_{1-x}Co_x(C_2O_4)\cdot 2H_2O$ ($x=0$, 0.05, 0.10, 0.15, 0.20, 0.25, 0.30) were prepared by adding 0.4 mol solutions of zinc and cobalt acetates with a 0.4 mol solution of oxalic acid. The precipitates were collected, washed with copious quantities of de-ionized water, and dried in air at 333 K. Powder x-ray diffraction confirmed that these oxalates form as single-phase materials. Heating the precursors at 1173 K for 15 min (with the samples being introduced into and removed from a preheated furnace) was identified as an appropriate condition for obtaining crystalline phases (as manifested in narrow x-ray linewidths) displaying high cobalt solubility. All the samples were moss green, becoming darker with increasing Co loading.

Powder x-ray diffraction patterns were acquired on a Scintag X2 diffractometer operating in the Bragg-Brentano geometry and employing Cu $K\alpha$ radiation. Data were step scanned using a step size of 0.02° in 2θ and subject to Rietveld profile analysis using the XND Rietveld code.[13] Magnetic data on three powder samples of $Zn_{1-x}Co_xO$ with $x=0.05$, 0.10, and 0.15 were acquired on a Quantum Design MPMS XL magnetometer.

For transmission electron microscopy (TEM), two samples with starting compositions of $x=0.15$ and $x=0.25$ were dispersed on carbon-coated copper grids and examined using a JEOL JEM 2000FX microscope equipped with an energy-dispersive x-ray (EDS) spectrometer.

III. COMPUTATIONAL METHODS

For the first-principles total energy calculations described here we used density functional theory based on pseudopotentials with localized atomic orbital basis sets. This method, implemented in the code SIESTA,[14–17] combines accuracy with small computational cost, particularly compared to other approaches such as plane-wave pseudopotential or all-electron methods.

We used standard scalar relativistic Troullier-Martins pseudopotentials[18] with nonlinear core corrections[19] and Kleinman-Bylander factorization.[20] We use the Ceperley-Alder local-spin-density exchange-correlation functional and include scalar relativistic effects for Co and Zn. For Zn, we include the $3d^{10}$ electrons in the valence manifold and construct the pseudopotential using a Zn^{2+} reference configuration with r_c of 2.0, 2.1, and 1.9 a.u. for the $4s$, $4p$, and $3d$ orbitals, respectively, and a partial core radius of 0.6 a.u. The eigenvalues and excitation energies of related configurations calculated with this pseudopotential agreed with the all-electron values to within 4 mRy, and the bulk lattice constants, atomic positions, and band structures (calculated using maximal basis sets to isolate pseudopotential effects from basis set effects) were in good agreement with all-electron values.[21] The Co pseudopotential, constructed from a $4s^1 3d^8$ reference configuration, r_c of 2.0 a.u. for all-valence orbitals, and a partial core cutoff of 0.75 a.u., had been previously tested for Co metal and shown to give good agreement with all-electron local-spin-density approximation (LSDA) lattice constants.[22] The oxygen pseudopotential was constructed from a $2s^2 2p^4$ reference configuration and r_c of 1.15 a.u. for each angular momentum channel and no core corrections. Eigenvalues and excitation energies for related atomic states agreed within 1 mRy of the all-electron values. This pseudopotential has also been tested extensively in calculations for bulk oxides.[23]

In localized orbital calculations, special care must be taken in the optimization of the basis set as described in Ref. 17. Here the number of basis functions and the confinement radii for each angular momentum component are used to achieve the required accuracy. Since the calculated structural and electronic properties of ZnO were largely unchanged on reducing the maximal basis to two unpolarized basis functions per orbital, we decided to use such a double-ζ basis for each Zn and O orbital. Since we are mainly interested in the magnetic properties of dilute systems which contain a small number of magnetic ions, we followed Ref. 24 in using a triple-ζ basis for the *d* orbitals on Co and a double-ζ basis for the other Co orbitals. Note that we can afford to use a triple-ζ basis for Co *d* since there are only a few Co ions in the unit cell. In contrast, the use of larger basis sets for Zn and O results in a dramatic increase of the size of the computations. For the Zn and Co confinement radii we chose the values from Ref. 24 of $r_c=6.0$, 6.0, and 5.0 a.u. for *s*, *p*, and *d* orbitals, respectively. These had been well tested for other transition metals, and repeats of these tests for Co and Zn gave similar accuracy. Combined with values of $r_c=5.5$ for O *s* and *p* orbitals, we obtained energy differences between ferromagnetic and antiferromagnetic states which agreed well with those for larger r_c values while maintaining a reasonable computation time.

Other details include a $4\times4\times3$ Monkhorst-Pack grid for 32-atom total energy calculations, with a $10\times10\times8$ interpolation for density of states calculations, a real space mesh cutoff of 180 Ry, and the neglect of nonoverlap interactions.

IV. RESULTS

A. Structure

In Fig. 1, we show powder x-ray diffraction data for the different $Zn_{1-x}Co_xO$ compositions. Points correspond to data and solid lines to Rietveld fits. Vertical markers at the top of the figures indicate expected peak positions for the wurtzite phase and for the spinel Co_3O_4 phase which emerges in the samples with high starting *x* values ($x=0.25$, 0.30). Solid lines through the points are the results of Rietveld analysis. In the case of the $x=0.25$ and $x=0.30$ samples, Rietveld analysis involved fitting two crystalline phases, wurtzite and spinel. The Rietveld fits provide convincing evidence that the samples are single phase up to

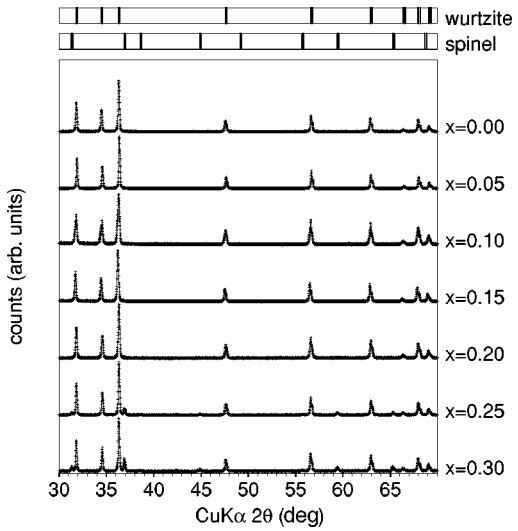

FIG. 1. Powder x-ray diffraction patterns of the different $Zn_{1-x}Co_xO$ (x indicated) displayed as points, with the Rietveld fit displayed as solid lines. The vertical markers at the top of the figure indicate expected peak positions for the wurtzite and spinel phases. The patterns for the $x=0.25$ and $x=0.30$ samples have been fitted to both phases in the Rietveld method.

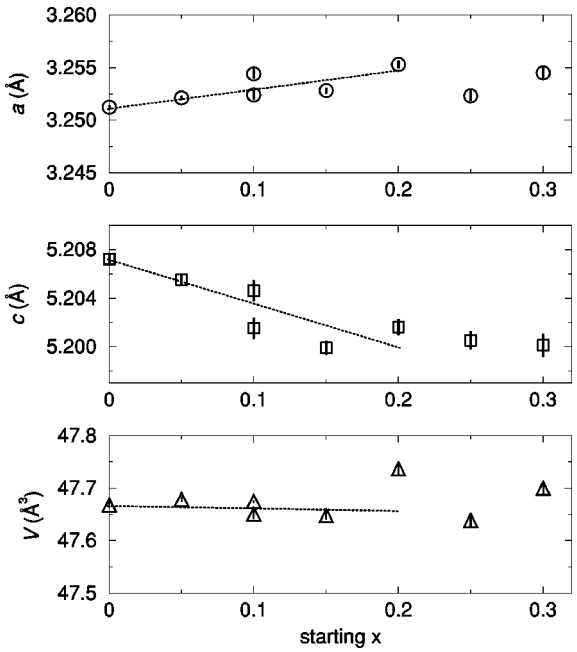

FIG. 2. Evolution of a and c cell parameters and unit cell volume of the hexagonal wurtzite phases of $Zn_{1-x}Co_xO$ as a function of starting x values. Vertical lines associated with the points are error bars from the Rietveld analysis and tend to be underestimates of the true error. For $x=0.10$, independent results from two separate samples are displayed. The dashed lines are guides to the eye.

an x value of 0.20. Due to the poor contrast between Co and Zn in x-ray diffraction (XRD), the analysis could not be used to refine the relative amounts of these ions in the wurtzite structure. Rietveld analysis also allowed the extraction of accurate cell parameters and, for the case of the $x=0.25$ and $x=0.30$ samples, a quantitative estimate[25] of the ratio of wurtzite and spinel phases. Such phase analysis indicated that the spinel phase incorporates a significant amount of zinc.

Figure 2 shows the evolution of the hexagonal a and c cell parameters, and the unit cell volume of the $Zn_{1-x}Co_xO$ samples, as a function of the starting values of x. The difference in radii between divalent, high-spin Co in tetrahedral coordination (0.58 Å) and divalent Zn in tetrahedral coordination (0.60 Å) (Ref. 26) is small. As a result, changes in cell parameters and cell volume with cobalt substitution are also small. Interestingly, while the substitution results in a decrease in the c parameter (in keeping with the smaller radius of Co^{2+}), the a parameter actually increases. Co^{3+} does not readily enter tetrahedral coordination. If the Co^{2+} ions were in an octahedral environment in the wurtzite structure, it would be signaled by a significant increase in the cell parameters since octahedral Co^{2+} has a radius between 0.65 Å (low spin) and 0.745 Å (high spin).[26]

Since x-ray diffraction is a ''bulk'' technique and is not always sensitive to small precipitates of a second phase, we have also studied two of the samples, $x=0.15$ and $x=0.25$, by transmission electron microscopy. These two samples flank the two sides of what XRD suggests to be the solubility limit for Co^{2+} in ZnO under the conditions presented here. Micrographs of the two samples are displayed in Figs. 3(a) and 3(b). The images corresponding to the $x=0.15$ samples [Fig. 3(a)] suggest single crystals with sizes in the 50–200 nm range. Although some defects are visible (indicated by arrows), the composition determined by EDS was uniform for this sample. TEM images of the $x=0.25$ sample [Fig. 3(b)], on the other hand, comprise larger particles with a high density of structural defects. The inhomogeneous contrast in the TEM images may reflect defects arising from the precipitation of the second (spinel) phase. EDS indeed suggested significant variations in the Zn:Co ratio between different particles.

B. Magnetism

From the structural studies, it is clear the $Zn_{1-x}Co_xO$ samples with $x=0.05$, 0.10, and 0.15 have Co^{2+} ions substituting uniformly for Zn^{2+} in the wurtzite lattice. The sample $x=0.25$ shows clear evidence for a second, spinel phase. The sample $x=0.20$ straddles the single-phase and two-phase regions of the metastable phase diagram, making it more difficult to state with certainty that it is single phase. A magnetic study of $Zn_{1-x}Co_xO$ samples with $x=0.05$, 0.10, and 0.15 was deemed appropriate. Plots of the molar magnetic susceptibility χ as a function of T for the three samples are displayed in Fig. 4(a). The traces from bottom to top correspond to $x=0.05$, $x=0.10$, and $x=0.15$. Data were acquired on warming in a field of 1000 Oe, after cooling in zero field (ZFC). Data taken on warming after field cooling (FC) displayed identical behavior.

Plots of the inverse molar susceptibility $1/\chi$ as a function of T are displayed in Fig. 4(b) as solid lines. This time, the bottommost trace corresponds to the $x=0.15$ sample, the middle trace to $x=0.10$, and the topmost trace to $x=0.05$. The high-temperature parts (between 300 and 400 K) of $1/\chi$

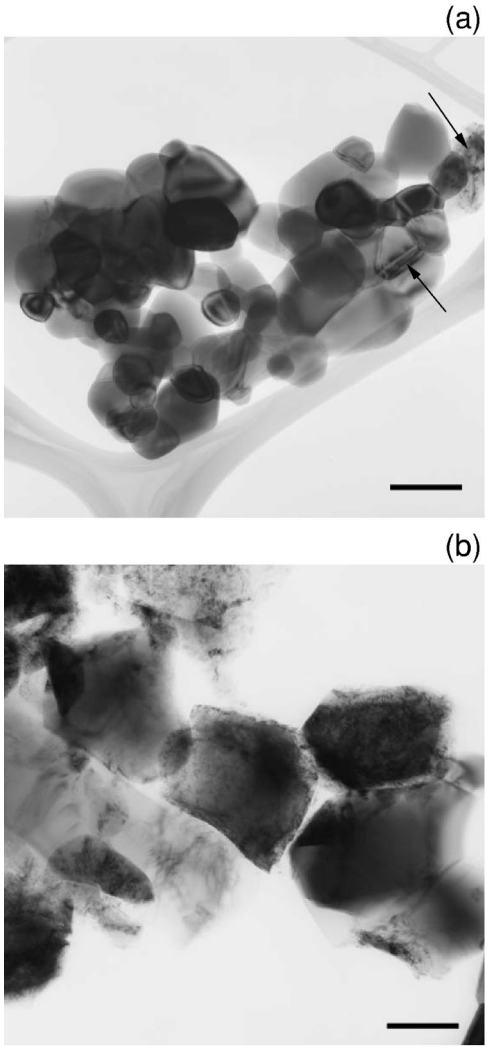

FIG. 3. TEM images of powders with the starting compositions $Zn_{1-x}Co_xO$ with $x=0.15$ [image (a)] and $x=0.25$ [image (b)]. The scale bars on the images correspond to 200 nm.

vs T display Curie-Weiss behavior and the data could be fitted to a straight line. These straight lines [dashed in Fig. 4(b)] have been extrapolated to the temperature axis to obtain values of the Curie-Weiss Θ, which is indicative of the nature and strength of coupling between magnetic ions in the lattice. For the $x=0.05$ sample, Θ is small and positive (≈ 20 K). For larger values of x—namely, $x=0.10$ and $x=0.15$—the sign of Θ becomes negative. The magnitudes are larger, due to the higher concentration of magnetic ions in the lattice and, therefore, shorter average distances between ions. The values of Θ are ≈ -60 and ≈ -90 K, respectively, for $x=0.10$ and $x=0.15$.

The Curie-Weiss fit permits calculation of the effective magnetic moment μ_{eff} per mole from the slope C in $\chi = C/(T-\Theta)$. C is related to μ_{eff} through $\mu_{\text{eff}} = \sqrt{(3k_B C)/N_A}$ where k_B is the Boltzmann constant and N_A the Avogadro number. From μ_{eff}, we calculate the number of unpaired electrons per formula unit of $Zn_{1-x}Co_xO$, using $\mu_{\text{eff}} = g\sqrt{J(J+1)}\mu_B$ where the Landé g factor is 1.54 for Co^{2+} (Ref. 27). The values of J have then been converted to

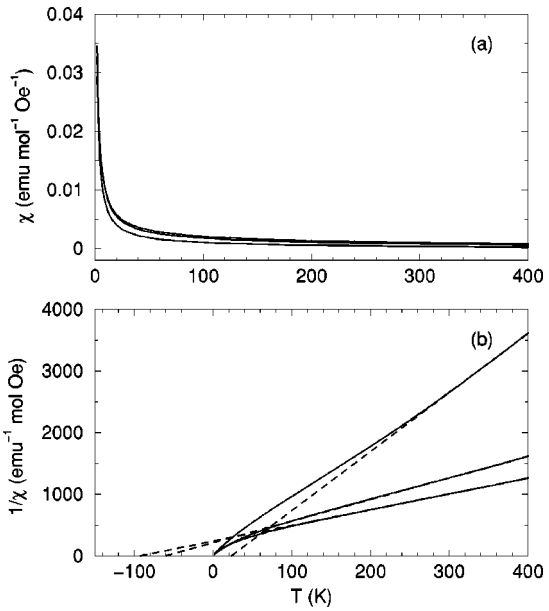

FIG. 4. (a) Susceptibility vs temperature of three samples of $Zn_{1-x}Co_xO$ (bottom to top are $x=0.05$, 0.10, and 0.15) acquired under a field of 1000 Oe. (b) The solid lines are inverse susceptibility as a function of temperature (top to bottom are $x=0.05$, 0.10, and 0.15) and the dashed lines are the corresponding Curie-Weiss fits to the data between 300 K and 400 K. The fits have been extrapolated to the point where they meet the temperature axis.

number of unpaired electrons per formula unit. This is plotted as a function of starting x for the different $Zn_{1-x}Co_xO$ in Fig. 5 as points. The dashed line corresponds to the *expected* values of the number of unpaired electrons per formula unit assuming all the cobalt in the structure exists as tetrahedral Co^{2+} in the high-spin d^7 configuration $e^4t_2^3$. The close correspondence between experiment and expectation supports our belief that sample stoichiometries, oxidation states, and homogeneity are as suggested by the formula $Zn_{1-x}Co_xO$ with $x=0.05$, 0.10, and 0.15.

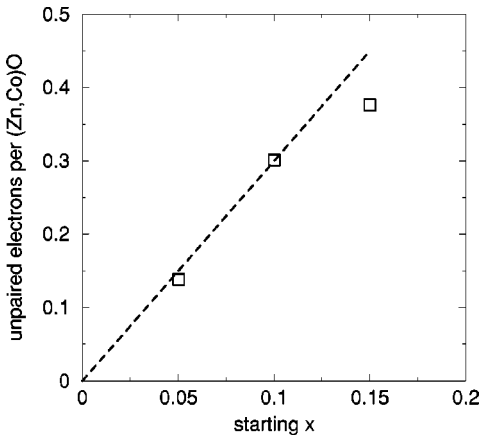

FIG. 5. Points show, for the different samples, the number of unpaired electrons per formula unit extracted from the effective magnetic moment, which in turn is obtained from the slope of the Curie-Weiss fit. The dashed line shows expected values assuming the starting formula $Zn_{1-x}Co_xO$ accurately describes the sample and that each cobalt atom is divalent with three unpaired electrons.

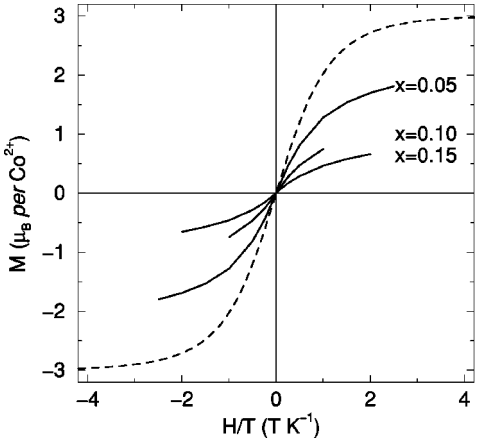

FIG. 6. Magnetization M per Co^{2+} atom in the sample, expressed in μ_B at a temperature of 2 K as a function of M/T. The dashed line is the Brillouin function for a Co^{2+} ion with three unpaired electrons, using a g value of 1.54.

Low-temperature (2 K) magnetization as a function of magnetic field scaled by the temperature is shown for the three samples in Fig. 6. Also shown for comparison is the Brillouin function (dashed trace) for a system with three unpaired spins and a g value of 1.54. It is immediately clear that none of the samples display any sort of *ferromagnetic* ordering or any evidence of hysteresis. The sample $x=0.05$, with the lowest concentration of magnetic ions, is the closest in its behavior to the Brillouin function, meaning that it is closest to being an ideal paramagnet with no magnetic interactions. When the concentration of magnetic ions in the lattice is larger (for larger starting values of x) and the average spacing between them is smaller, the deviation from ideal paramagnetism is greater. The magnetization of the $x=0.10$ and $x=0.15$ samples tends to saturate to smaller values, but the saturation behavior for all three samples commences at approximately the same value of H/T as the Brillouin function.

C. Computation

We begin by constructing a 32-atom wurtzite structure supercell of ZnO (16 ZnO formula units). The supercell is formed by doubling the conventional four-atom wurtzite structure along each axis, adopting the experimental lattice constant. This gives the lattice vectors

$$\begin{pmatrix} 1/2 & -\sqrt{3}/2 & 0 \\ 1/2 & \sqrt{3}/2 & 0 \\ 0 & 0 & c/a \end{pmatrix},$$

where a and c refer to the wurtzite cell parameters with $a=12.28$ a.u. and $c/a=1.6024$. Densities of state for this wurtzite supercell are displayed in Fig. 7(a). Zn d states are found concentrated within a region centered around -7 eV with a dispersion of about 2 eV. Oxygen p states are concentrated in the region between -6 eV and -2 eV. There is some Zn $3d$–O $2p$ covalency as has been previously

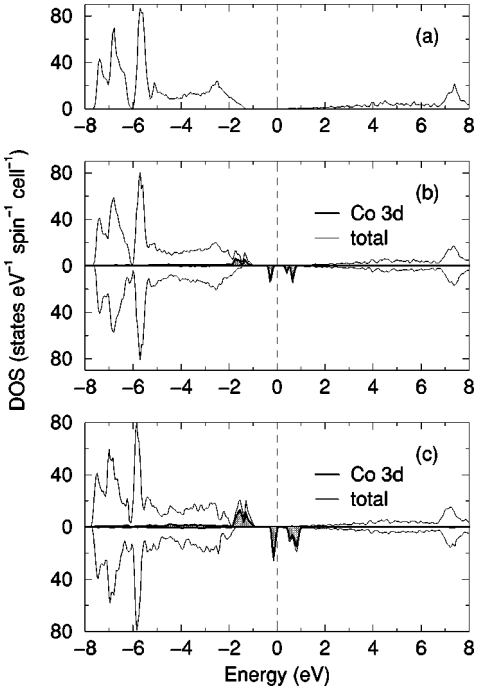

FIG. 7. Densities of state (a) for a ZnO supercell ($2\times2\times2$ wurtzite ZnO cells), (b) of Co d states (shaded) and total states for ferromagnetic $Zn_{15}CoO_{16}$, and (c) of Co d states (shaded) and total states for ferromagnetic $Zn_{14}Co_2O_{16}$. In panels (b) and (c), the upper halves display spin $\uparrow$ states while the lower halves display $\downarrow$ states.

noted.[28] The densities of state and band gap of pristine ZnO presented here reproduce earlier high-level band structure results.[28]

When one Co atom is included in each supercell, ordering of spins is forced to be ferromagnetic. The concentration of Co ions is 6.25% and the formula of the compound is $Zn_{15}CoO_{16}$. The magnetic moment per unit cell is calculated to be $3.10\mu_B$, close to the value of $3.0\mu_B$ predicted for purely ionic Co^{2+} with three unpaired electrons.

The density of states for such a 32-atom unit cell containing a single Co atom is shown in Fig. 7(b). The density of states is very similar to pristine ZnO, except for the well-defined and -localized Co states (shaded gray, with a thick solid line) within the band gap region. Comparing Figs. 7(a) and 7(b), it is seen that the spin polarization of the Co atom barely affects Zn and O states.

With an odd number of electrons and in the absence of any spin polarization, $Zn_{15}CoO_{16}$ should be a metal within the density functional theory local density approximation (DFT-LDA). The electronic configuration of the d^7 tetrahedral system would be e^4, t_2^3 with the Fermi energy lying in the half-filled t_2 manifold (e comprises $d_{x^2-y^2}$ and d_{z^2} while t_2 comprises d_{xy}, d_{yz}, and d_{xz}). When spin polarization is switched on, as is the case here, insulating ground states can be obtained within the LSDA provided the different spin directions are separated by a gap. We observe that the density of states (DOS) shown in Fig. 7(b) is indeed gapped at the Fermi energy.

The Fermi energy is found to lie between two spin $\downarrow$

TABLE I. Relative stabilization (in meV) of the different magnetic ground states.

$Zn_{14}Co_2O_{16}$		
	FM	AFM
"Near"	−1	0
"Separated"	−4	0
$Zn_{13}\square Co_2O_{16}$		
"Near"	−60	0
"Separated"	−60	0
$Zn_{14}Co_2O_{15}\square$		
"Near"	0	−1
"Separated"	0	−4

states. In order to understand this, we must recognize that the exchange splitting (between ↑ and ↓ states) in Fig. 7 is almost 2 eV, while the crystal field splitting is much less than 1 eV. The d^7 configuration is therefore

$$e^2(\uparrow),\ t_2^3(\uparrow),\ e^2(\downarrow)||t_2^0(\downarrow).$$

The small crystal field splitting and large exchange splitting is consistent with what one expects for a tetrahedral, oxide ligand field, and three unpaired electrons.

It is important to note that the gap is, in some sense, fortuitous. If the crystal field or exchange splitting were any smaller in comparison with the bandwidths or the electronic configuration did not correspond to high-spin, tetrahedral Co^{2+}, we would likely obtain a metallic ground state within the LSDA. Indeed, *ab initio* electronic structure calculations of Sato and Katayama-Yoshida[4] yield a metallic, magnetic ground state for Zn_3CoO_4. However, since the compounds discussed here have very narrow bands, extensions to LSDA methods, such as LDA+U or self-interaction corrections,[29] would restore the band gap even in systems that within LSDA are found to be metallic.

When two Co atoms are included in a 32-atom unit cell (giving a 12.5% substituent concentration with the formula $Zn_{14}Co_2O_{16}$), a number of different magnetic and positional arrangements are possible. Here we adopt two different pairs of Co positions: a "near" configuration, in which the Co ions in the same unit cell are separated by a single O ion, and a "separated" configuration, in which they are connected via -O-Zn-O- bonds. The densities of state in Fig. 7(c) are displayed for a system where the two Co atoms are "near" and their spins are parallel (ferromagnetic). For both "near" and "separated" configurations we have calculated the relative energies of the ferromagnetic (FM) and antiferromagnetic (AFM) spin alignments. We find for both configurations that the energies of the FM and AFM configurations are very close, with the FM being slightly lower (the energy of the "separated" FM configuration is 4 meV lower than that of the "separated" AFM configuration and for the "near" configuration FM is only 1 meV lower than the AFM).

We have modeled hole doping in our system by removing a Zn atom from the unit cell of $Zn_{14}Co_2O_{16}$ to form $Zn_{13}\square Co_2O_{16}$ with □ representing the vacancy (see Table I). Such *p*-type doping strongly stabilizes the FM state. In both the separated and near configurations the FM state is now 60 meV lower in energy than the AFM state. In contrast, if the vacancy is created on the anion site (O atom replaced by a □), the resulting *n* doping stabilizes the AFM state. In the *n*-doped "separated" configuration, the AFM state is now 4 meV lower in energy than the FM, and for the "near" configuration the AFM state is 1 meV lower than the FM.

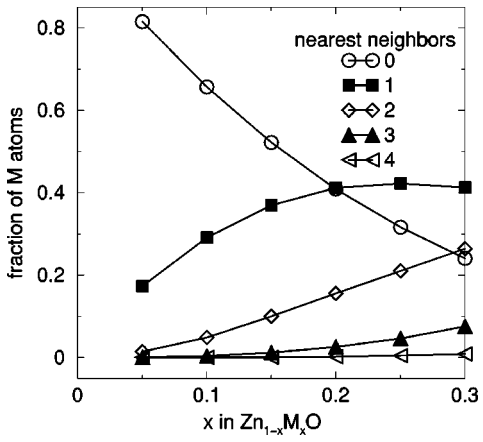

FIG. 8. Fraction of the total number of *M* atoms that have 0, 1, 2, 3, and 4 *M* nearest neighbors in $Zn_{1-x}M_xO$, assuming that *M* substitutes Zn in a completely random manner.

The very small stabilization of the ferromagnetic ground state in $Zn_{14}Co_2O_{16}$ is in agreement with the more approximate KKR calculations of Sato and Katayama-Yoshida,[3,4] who obtain fractions of mRy stabilization of the ferromagnetic ground state in 10% Co-substituted ZnO. For the hole- and electron-doped systems, their results are quite different from ours. For example, they find that electron doping induces ferromagnetic coupling. The manner in which they achieve such doping is different from what we have done here, so comparisons may not be valid. We do not choose to interpret small (<10 meV) differences in the energies of the different ground states as being significant. The most striking result of our calculations is that robust ferromagnetism in $Zn_{1-x}Co_xO$ is only possible in the presence of substantial hole doping.

V. DISCUSSION

The DFT calculations suggest that energy differences between ferromagnetic and antiferromagnetic arrangements in all cases except when there is cation vacancy (hole doping) are small, of the order of a few meV. However, a trend is observed that helps in the interpretation of the magnetic data—namely, when the magnetic atoms are separated, the tendency to ferromagnetic ordering is enhanced. To recapitulate, while the $x=0.05$ sample showed evidence for ferromagnetic interactions between Co^{2+} (with a positive Curie-Weiss Θ of $\approx$20 K), the $x=0.10$ and $x=0.15$ samples suggest nearest-neighbor antiferromagnetism, with Θ values around −60 K and −90 K. To interpret these, we consider in Fig. 8, the fraction of Co ions (or M ions in general) in the

wurtzite lattice (ignoring the anion) that have other Co(M) nearest neighbors, as a function of x. When $x=0.05$, we observe that approximately 80% of Co^{2+} have no nearest-neighbor Co^{2+}. This means that most of the magnetism arises from coupling through intervening Zn and therefore corresponds to the ''separated'' case. As x increases, the fraction of Co^{2+} that have nearest-neighbor Co^{2+} grows rapidly, and the dominant magnetic interaction (which is also stronger because the distances are smaller) is due to the ''near'' case.

The inverse susceptibility traces for all three samples extrapolate to the origin, suggesting divergence of χ at $T=0$ K. At first, this is puzzling, given that Θ changes sign on going from $x=0.05$ to $x=0.10$ and 0.15. However, we recognize that all three samples can be thought of as comprising two kinds of magnetic ions, ones that are paired—i.e., have nearest neighbors—and ones that are ''isolated'' and do not. It is the ''isolated'' ions that act as paramagnets and for which $\chi\rightarrow\infty$ as $T\rightarrow 0$. A recent study by Kolesnik, Dabrowski, and Mais[30] of $Zn_{1-x}Mn_xO$ also shows such a downturn ($1/\chi\rightarrow 0$ as $T\rightarrow 0$) for $x=0.05$, 0.10, 0.15, and 0.20.

The smaller 2 K saturation moments at higher Co^{2+} concentrations (for $x=0.10$ and $x=0.15$) arise because as x increases, a larger fraction of the Co^{2+} are coupled antiferromagnetically in pairs (between nearest neighbors). The saturation behavior is from the ''isolated'' Co^{2+} that have no nearest-neighbor Co^{2+}, and these form larger fractions of the magnetic ions when x is smaller.

ACKNOWLEDGMENTS

A.S.R. is supported by the National Science Foundation IGERT program under Award No. DGE-9987618. This work was partially supported by the MRL program of the National Science Foundation under Award No. DMR00-80034 and in part by the Department of Energy, Grant No. DOE DE-FG03-02ER45986. We thank James O'Brien of Quantum Design for the magnetic data. N.A.S. thanks the Earth Sciences Department at Cambridge University for their hospitality during the sabbatical leave in which the calculations were performed. R.S. would like to acknowledge a start-up grant from the Dean, College of Engineering, UCSB.

*Electronic address: aditi@engineering.ucsb.edu
†Electronic address: nicola@mrl.ucsb.edu
‡Electronic address: stemmer@mrl.ucsb.edu
§Electronic address: seshadri@mrl.ucsb.edu

[1] D.D. Awschalom, M.E. Flatté, and N. Samarth, Sci. Am. (Int. Ed.) **286**, 66 (2002); S. Das Sarma, Am. Sci., **89**, 516 (2001); N. A. Spaldin, *Magnetic Materials, Fundamentals and Device Applications* (Cambridge University Press, Cambridge, England, 2003).
[2] T. Dietl, H. Ohno, F. Matsukura, J. Cibert, and D. Ferrand, Science **287**, 1019 (2000).
[3] K. Sato and H. Katayama-Yoshida, Jpn. J. Appl. Phys., Part 2 **39**, L555 (2000).
[4] K. Sato and H. Katayama-Yoshida, Phys. Status Solidi B **229**, 673 (2002).
[5] K. Ando, H. Saito, Z. Jin, T. Fukumura, M. Kawasaki, Y. Matsumoto, and H. Koinuma, J. Appl. Phys. **89**, 7284 (2001).
[6] K. Ando, H. Saito, Z. Jin, T. Fukumura, Y. Matsumoto, A. Ohtomo, M. Kawasaki, and H. Koinuma, Appl. Phys. Lett. **78**, 2700 (2001).
[7] K. Ueda, H. Tabata, and T. Kawai, Appl. Phys. Lett. **79**, 988 (2001).
[8] J.H. Kim, H. Kim, D. Kim, Y.E. Ihm, and W.K. Choo, Physica B **327**, 304 (2003); J.H. Kim, W.K. Choo, H. Kim, D. Kim, and Y.E. Ihm, J. Korean Phys. Soc. **42**, S528 (2003).
[9] Z.-W. Jin, T. Fukumura, K. Hasegawa, Y.-Z. Yoo, K. Ando, T. Sekiguchi, P. Ahmet, T. Chikyow, T. Hasegawa, H. Koinuma, and M. Kawasaki, J. Cryst. Growth **237-239**, 548 (2002).
[10] S.-W. Lim, D.-K. Hwang, and J.-M. Myoung, Solid State Commun. **125**, 231 (2003).
[11] S.J. Pearton, C.R. Abernathy, M.E. Overberg, G.T. Thaler, D.P. Norton, N. Theodoropoulou, A.F. Hebard, F. Ren, J. Kim, and L.A. Boatner, J. Appl. Phys. **93**, 1 (2003).
[12] V. Jayaram and B. Sirisha Rani, Mater. Sci. Eng., A **304-306**, 800 (2001).
[13] J.-F. Bérar and P. Garnier, computer code XND, 1992, available from the website at http://www.ccp14.ac.uk
[14] P. Ordejón, D. Sánchez-Portal, E. Artacho, and J.M. Soler, computer code SIESTA, Spanish Initiative for Electronic Simulations with Thousands of Atoms.
[15] D. Sánchez-Portal, P. Ordejón, E. Artacho, and J.M. Soler, Int. J. Quantum Chem. **65**, 453 (1997) and references therein.
[16] P. Ordejón, Phys. Status Solidi B **217**, 335 (2000).
[17] E. Artacho, D. Sanchez-Portal, P. Ordejón, A. García, and J.M. Soler, Phys. Status Solidi B **215**, 809 (1999).
[18] N. Troullier and J.L. Martins, Phys. Rev. B **43**, 1993 (1991).
[19] S.G. Louie, S. Froyen, and M.L. Cohen, Phys. Rev. B **26**, 1738 (1982).
[20] L. Kleinman and D.M. Bylander, Phys. Rev. Lett. **48**, 1425 (1982).
[21] A. Dal Corso, M. Posternak, R. Resta, and A. Baldereschi, Phys. Rev. B **50**, 10 715 (1994).
[22] K.F. Goto, N.A. Spaldin, and S. Sanvito (unpublished).
[23] J. Junquera and P. Ghosez, Nature (London) **422**, 506 (2003).
[24] S. Sanvito, P. Ordejón, and N.A. Hill, Phys. Rev. B **63**, 165206 (2001).
[25] G.W. Brindley, Philos. Mag. **36**, 347 (1945).
[26] R.D. Shannon and C.T. Prewitt, Acta Crystallogr., Sect. B: Struct. Crystallogr. Cryst. Chem. **25**, 925 (1969); R.D. Shannon, Acta Crystallogr., Sect. A: Cryst. Phys., Diffr., Theor. Gen. Crystallogr. **32**, 751 (1976).
[27] B.D. Cullity, *Introduction to Magnetic Materials* (Addison-Wesley, Reading, MA, 1972).
[28] N.A. Hill and U.V. Waghmare, and N.A. Hill, Phys. Rev. B **62**, 8802 (2000).
[29] A. Filippetti and N.A. Spaldin, Phys. Rev. B **67**, 125109 (2003).
[30] S. Kolesnik, B. Dabrowski, and J. Mais, J. Supercond. **15**, 251 (2002).